Non-periodic tessellations with unit and non-unit Pisot inflation factors

2005 J. Phys. A: Math. Gen. 38 6525

(http://iopscience.iop.org/0305-4470/38/29/008)

INSTITUTE OF PHYSICS PUBLISHING JOURNAL OF PHYSICS A: MATHEMATICAL AND GENERAL

J. Phys. A: Math. Gen. **38** (2005) 6525–6543 doi:10.1088/0305-4470/38/29/008

Non-periodic tessellations with unit and non-unit Pisot inflation factors

Juan García Escudero[1] **and Javier García García**[2]

[1] Departamento de Matemáticas, Universidad Politécnica de Madrid, EUIT Agrícolas, Ciudad Universitaria, 28040 Madrid, Spain
[2] Departamento de Física, Universidad de Oviedo, 33007 Oviedo, Spain

Received 25 October 2004, in final form 19 April 2005
Published 6 July 2005
Online at stacks.iop.org/JPhysA/38/6525

Abstract

Non-periodic planar patterns generated by deterministic inflation rules are described. Several types of patterns with both unit and non-unit Pisot numbers as inflation factors are formed by triangular prototiles. When the inflation factor is the silver mean, the patterns can be obtained by superimposing two subpatterns and some of them can be converted into face-to-face patterns. The geometric constructions corresponding to 12-fold symmetry are also studied. The Fourier transform of point masses, placed in vertex positions of the transformed subpatterns, exhibit two-fold, four-fold and six-fold symmetries, although the peaks with highest intensities are situated in rings with apparent octagonal and dodecagonal symmetries.

PACS numbers: 61.44.Br, 61.50.Ah

1. Introduction

The discovery in 1984 by Shechtman, Blech, Gratias and Cahn [1] and by Ishimasa, Nissen and Fukano [2] of quasicrystal phases in Al–Mn and Cr–Ni alloys, respectively, has motivated research on abstract tilings in order to understand the structures of such materials [3, 4].

Geometric constructions for the derivation of substitution rules for planar tilings with odd symmetries not divisible by three have been given in [5]. On the other hand, several types of simple and composite triangle tilings have been generated in [6–8], by extending the geometric constructions in order to study symmetries with experimental confirmation, namely octagonal, decagonal and dodecagonal. Other types of geometric constructions produce hexagonal and octagonal non-deterministic structures [9].

A description in terms of word sequences in Lindenmayer systems allows us to study in an efficient way the possible tile orientations. The results of our study [10, 11] show that for four-fold symmetry it is possible to separate the original patterns into two subpatterns. By superimposing these subpatterns, which are not face to face, we can get the original ones. For

this case, it is possible to transform the subpatterns into face-to-face patterns generated by substitution rules. In this paper, we review these results and extend them to other symmetries with interest from an experimental point of view.

Pisot numbers play a significant role in the theory of quasicrystals. They are related with the existence of Bragg peaks in the diffraction patterns. When a tiling is used for the description of a real quasicrystal, the prototiles are decorated with mass distributions which represent the atomic positions. In order to understand the nature of the mathematical diffraction of the corresponding point sets, it is important to know if the tiling scaling factor is a Pisot number. In this work, we study triangle patterns with octagonal (section 2) and dodecagonal (section 3) symmetries. They have unit and non-unit Pisot numbers as inflation factors. For the dodecagonal pattern corresponding to a unit Pisot number, we compute the intensities for the Bragg peaks (section 3). For the octagonal case, the same prototile set can also be used for the generation of two types of patterns, derived in [6], with the silver ratio as inflation factor. In relation with one of the patterns we showed in [11] that a non-face-to-face subpattern, containing half of the orientations, can be converted into face-to-face patterns with four-fold symmetry. We treat this case with more detail in section 4 and we show that this result can also be generalized to two-fold (section 4) and six-fold symmetries (section 5). When the subpatterns are transformed into face-to-face structures, the complexity and number of prototiles increases in relation with the original triangle patterns. The Fourier analysis of the transformed subpatterns show binary, tetragonal and hexagonal symmetries, although the peaks with highest intensities show apparent noncrystallographic eight-fold and twelve-fold symmetries.

2. Octagonal patterns

The patterns studied in this section have triangles as prototiles. Their edges A, B, C, D have lengths $l_A = s_1, l_B = s_2, l_C = s_3, l_D = s_4$, where $s_\nu = \sin(\nu\pi/8)$. Arrows are placed on the edges. For a given triangle, the edges are labelled 0 or 1, depending on whether the arrow orientation is anticlockwise or clockwise, respectively.

The letters $a_m, \bar{a}_m, b_m, c_m, d_m, e_m, \bar{e}_m$ represent the prototiles (table 1 and figure 1(*a*)), where $\mathcal{T}(X, Y, Z)$ is a triangular tile with edges X, Y, Z placed anticlockwise and the index $m \in Z_{16}$ denotes relative orientation. The tile $\mathcal{T}(X, Y, Z)$, with the edge Z placed on the positive x-axis, corresponds to the index 1. The oriented tile with index m is obtained by a rotation of $\pi(m-1)/8$ through the leftmost vertex.

In what follows the mirror image of the word w is denoted by $\mathrm{Mir}(w)$, the projection of L^j into L by $P(L^j)$ and t is the map $t\big(L_1^i \ldots L_2^j L_3^k\big) = L_1^{i+1} \ldots L_2^{j+1} L_3^{k+1}$ with $i, j, k \in Z_2$. If we choose anticlockwise orientation, the substitution rules for the edges $X \longmapsto \phi_-[X]$ in the first type of patterns we consider are given in table 1. Observe

$$\phi_-(L^i) = \mathrm{Mir}(t(\phi_-(L^{i+1}))), \tag{1}$$

and $\phi_-(D) = \mathrm{Mir}(t(\phi_-(D)))$, therefore we do not need to put an arrow on the edge D.

Only L^0 and L^1 are common edges of two adjacent tiles. Therefore, the fact that the tilings are face to face is equivalent to

$$P\big(\phi_-^n(L^i)\big) = \mathrm{Mir}\big(P\big(\phi_-^n(L^{i+1})\big)\big), \tag{2}$$

which is a consequence of equation (1). The relations given by equation (2) are also valid for all the patterns considered in this work.

The patterns corresponding to the edge inflation rules ϕ_- given in table 1 can be described in terms of substitutional sequences. A 0L system is a triple $G = \{\Sigma, h, \omega\}$ where Σ is an

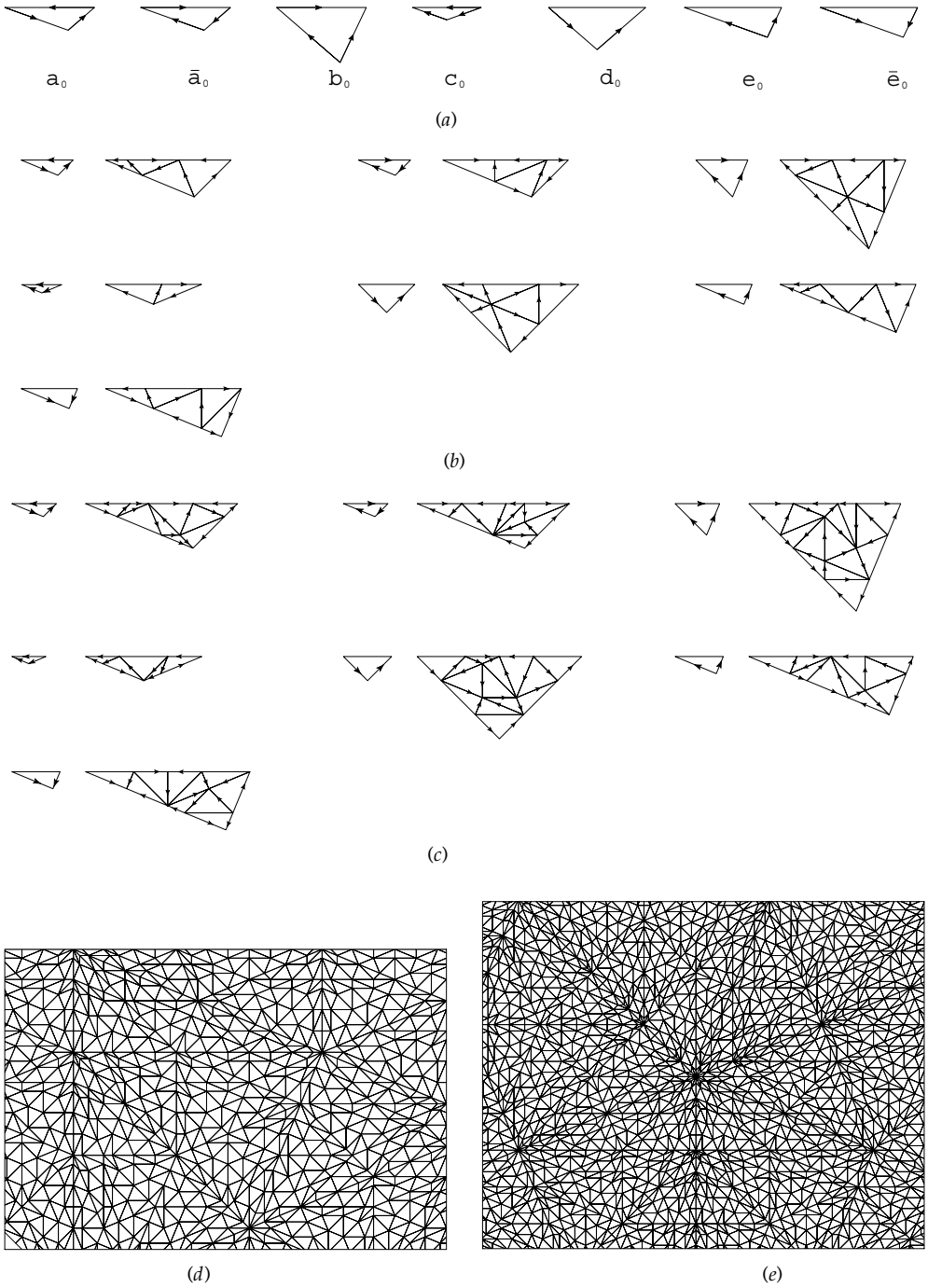

Figure 1. The patterns Til(8, −) and Til(8, +). (*a*) The prototile set. (*b*) Substitution rules for Til(−). (*c*) The substitution atlas for Til(8, −). (*d*) A portion of Til(8, −). (*e*) A portion of Til(8, +).

Table 1. Prototiles and edge inflation rules for Til(8, −) and Til(8, +). Even iterations of $\phi_-(\phi_+)$ generate Til(8, −)(Til(8, +)) (see figure 1).

Tiles			
a_m	$\bar{a}_m$	b_m	c_m
$\mathcal{T}(B^0, A^0, C^0)$	$\mathcal{T}(B^1, A^1, C^1)$	$\mathcal{T}(C^1, B^0, C^1)$	$\mathcal{T}(A^1, A^1, B^0)$
d_m	e_m	$\bar{e}_m$	
$\mathcal{T}(B^0, B^0, D)$	$\mathcal{T}(C^1, A^0, D)$	$\mathcal{T}(C^0, A^1, D)$	
Edge inflation rules			
ϕ_-:			
A^0	B^0	C^0	D
B^1	A^1C^0	DB^0	C^0C^1
A^1	B^1	C^1	
B^0	C^1A^0	B^1D	
ϕ_+:			
A^0	B^0	C^0	D
B^0	C^1A^0	B^1D	C^0C^1
A^1	B^1	C^1	
B^1	A^1C^0	DB^0	

alphabet, h is a finite substitution on Σ into the set of subsets of Σ^* and ω is the axiom. G is called a D0L system if $\#(h(x)) = 1$, for every x in Σ. The alphabet is

$$\Sigma = \{a_m, \bar{a}_m, b_m, c_m, d_m, e_m, \bar{e}_m, \widetilde{a}_m, \widetilde{\bar{a}}_m, \widetilde{b}_m, \widetilde{c}_m, \widetilde{d}_m, \widetilde{e}_m, \widetilde{\bar{e}}_m, (,)\}, \tag{3}$$

with $m \in Z_{16}$. It contains two parentheses (,) and letters of types t_i and $\widetilde{t_i}$ representing mirror images.

Every element belonging to Σ representing a tile can be used as an axiom. The set of production rules h_- is

$$\begin{aligned}
&a_m \longmapsto (\Phi_-[a_m]) = (c_m a_{m+7} \widetilde{d}_m)\\
&\bar{a}_m \longmapsto (\Phi_-[\bar{a}_m]) = (e_{m-6} \bar{a}_{m+9} \widetilde{\bar{a}}_{m+1})\\
&b_m \longmapsto (\Phi_-[b_m]) = ((\widetilde{d}_m b_{m+7} \widetilde{b}_{m+11}) \widetilde{e}_{m+6})\\
&c_m \longmapsto (\Phi_-[c_m]) = (a_m c_{m+9})\\
&d_m \longmapsto (\Phi_-[d_m]) = ((\widetilde{a}_m d_{m+7} \widetilde{b}_m) \bar{e}_{m+15})\\
&e_m \longmapsto (\Phi_-[e_m]) = (\bar{a}_m e_{m+7} \widetilde{b}_{m+6})\\
&\bar{e}_m \longmapsto (\Phi_-[\bar{e}_m]) = (\widetilde{\bar{e}}_{m+7} \bar{e}_{m+9} d_{m+1})\\
&) \longmapsto)\\
&(\longmapsto (
\end{aligned} \tag{4}$$

The geometric interpretation of the words sequences allows us to reconstruct the tiling from the words. In the word $((\widetilde{d}_m b_{m+7} \widetilde{b}_{m+11}) \widetilde{e}_{m+6})$, if two letters follow one another inside parentheses, the corresponding oriented triangles are glued face to face in a unique way. The oriented trapezoid $(\widetilde{d}_m b_{m+7} \widetilde{b}_{m+11})$ is also glued face to face with the oriented triangle $\widetilde{e}_{m+6}$. Iteration of the production rules generates words with increasing length representing the tiling growth.

In this work we are interested in patterns with a Pisot number (algebraic integer greater than 1, with the remaining roots of its minimal polynomial less than 1 in absolute value) as inflation factor. By iterating the inflation rules given by equation (4), a class of face-to-face

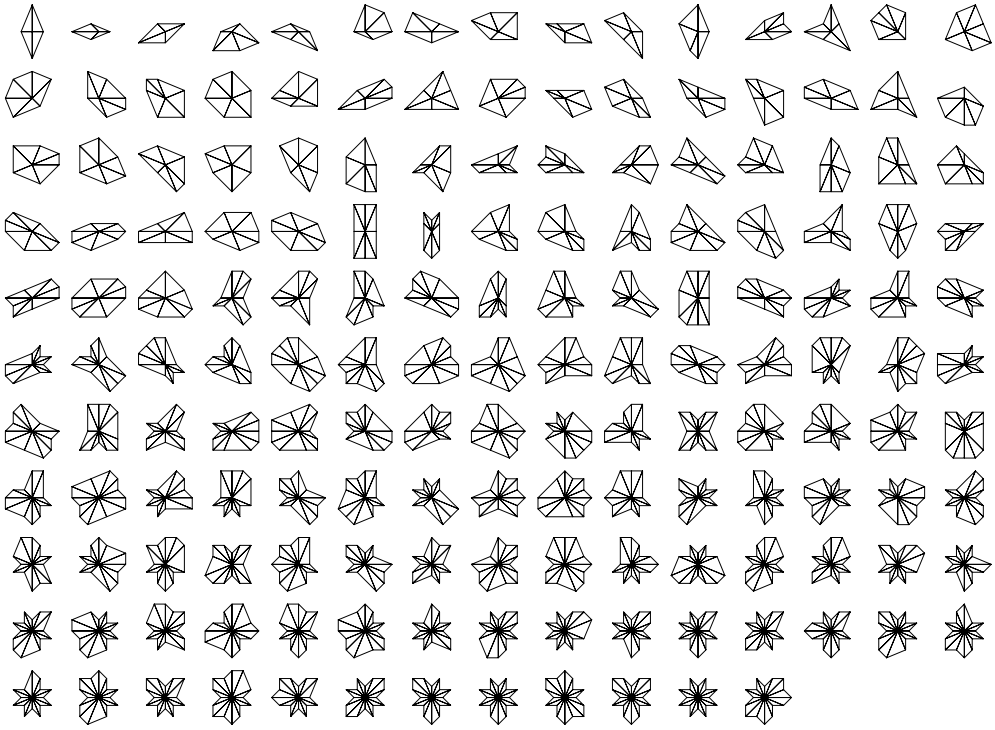

Figure 2. Vertex configurations of Til(8, +).

patterns is obtained. Although their inflation factor is not a Pisot number, we can obtain Pisot self-similar tilings Til(8, −) by considering the inflation rules $\Psi_-(t_i) = \Phi_-^2(t_i)$. The inflation factor is the Pisot number $(s_2/s_1)^2$, highest root of $x^2 - 4x + 2$. The substitution rules for the tiles can be seen in figure 1(*c*) and a portion of the pattern is shown in figure 1(*d*). It is possible to get other patterns with the same inflation factor s_2/s_1 and edge substitution rules $\phi_+(L^i) = \mathrm{Mir}(t(\phi_-(L^i)))$ (see table 1). A part of the Pisot pattern Til(8, +), generated by the inflation rules $\Psi_+(t_i) = \Phi_+^2(t_i)$, can be seen in figure 1(*e*)

A first idea about the patterns complexity is obtained by analysing the possible vertex configurations. In figure 2, we can see the 162 vertex configurations of Til(8, +), which appear in the iteration level $n = 5$ and, if we do not take into account the different arrowings, no new vertex configuration appears in $n = 6$. The 37 vertex configurations of Til(8, −) appear already in the third inflation step.

The same prototile set (figure 1(*a*)) was used in [6] for the generation of Til(−) and Til(+), which are self-similar patterns with the same scaling factor as the Ammann–Benker tiling, namely, s_3/s_1 (the silver ratio). The substitution atlas for Til(−) can be seen in figure 1(*b*). These patterns will be considered again in section 4, where we will show that they can be obtained by superimposing two structures.

3. Patterns with 12-fold symmetry

In this section, we introduce two types of dodecagonal patterns denoted by Til(12*a*) and Til(12*b*). We follow a procedure analogous to section 2. First, we introduce patterns with

Table 2. Prototiles and edge inflation rules for Til(12a) and Til(12b). Even iterations of $\phi_a(\phi_b)$ generate Til(12a)(Til(12b)) (see figure 3).

Tiles					
a_m	b_m	c_m	d_m	e_m	f_m
$\mathcal{T}(B^1, A^1, C^1)$	$\mathcal{T}(C^1, A^0, D^0)$	$\mathcal{T}(D^1, B^0, F)$	$\mathcal{T}(C^0, B^1, E^0)$	$\mathcal{T}(E^1, A^1, F)$	$\mathcal{T}(D^0, C^0, E^1)$
Edge inflation rules					
ϕ_a:					
A^0	B^0	C^0	D^0	E^0	F
B^0	A^1C^0	D^1B^0	E^0C^1	D^0F	E^1E^0
ϕ_b:					
A^0	B^0	C^0	D^0	E^0	F
D^1	E^0C^1	B^1D^0F	$A^1C^0E^1E^0$	$D^0FD^1B^0$	$C^0E^1E^0C^1$

a non-Pisot inflation factor and then we see that the even iterations give Pisot patterns. In table 2, the prototiles are represented by letters of type x_m. The edge lengths are in this case $A = s_1, B = s_2, C = s_3, D = s_4, E = s_5, F = s_6$ where $s_v = \sin(v\pi/12)$. The basic substitution rules ϕ_a for the edges can also be seen in table 2.

The alphabet for the grammar descriptions of Til(12a) and Til(12b) is

$$\{a_m, b_m, c_m, d_m, e_m, f_m, \widetilde{a}_m, \widetilde{b}_m, \widetilde{c}_m, \widetilde{d}_m, \widetilde{e}_m, \widetilde{f}_m, (,)\}$$

with $m \in Z_{24}$. The oriented tiles t_i and $\widetilde{t_i}$ are obtained by a rotation of $\pi(i-1)/12$ through the left most vertex. The set of production rules for a class of face-to-face patterns is

$$\begin{aligned}
&a_m \longmapsto (\Phi_a[a_m]) = (b_m a_{m+13} \widetilde{a}_{m+1}) \\
&b_m \longmapsto (\Phi_a[b_m]) = (a_m b_{m+11} c_m) \\
&c_m \longmapsto (\Phi_a[c_m]) = ((d_m c_{m+13} b_m) \widetilde{c}_{m+1}) \\
&d_m \longmapsto (\Phi_a[d_m]) = ((c_m d_{m+11} e_{m+23}) f_m) \\
&e_m \longmapsto (\Phi_a[e_m]) = (\widetilde{e}_{m+11} e_{m+13} d_{m+1}) \\
&f_m \longmapsto (\Phi_a[f_m]) = ((\widetilde{f}_{m+9} f_{m+13} d_m) \widetilde{f}_{m+1}) \\
&) \longmapsto) \\
&(\longmapsto (.
\end{aligned} \tag{5}$$

The patterns Til(12a) are generated by applying the inflation rules $\Psi_a(t_i) = \Phi_a^2(t_i)$ which are represented in figure 3(a). A part of the pattern can be seen in figure 3(b). The inflation factor is now the Pisot number $(s_2/s_1)^2$, highest root of $x^2 - 4x + 1$.

A different type of inflation rule for the same prototile set can be seen in figure 3(c). The edge inflation rules ϕ_b are described in table 2. The production rules Φ_b for the corresponding grammar (figure 3(c)) are

$$\begin{aligned}
&a_n \longmapsto (\tilde{a}_{n+11} \tilde{b}_n \tilde{c}_{n+11} \tilde{d}_n) \\
&b_n \longmapsto (\tilde{e}_{n+11} e_{n+13} d_{n+1} c_{n+14} \tilde{c}_{n+2} \tilde{b}_{n+15}) \\
&c_n \longmapsto (f_{n+15} \tilde{f}_{n+11} f_{n+23} d_{n+10} c_{n+23} b_{n+10} a_{n+23} \tilde{a}_{n+11} \tilde{b}_n \tilde{c}_{n+11} \tilde{d}_n) \\
&d_n \longmapsto (\tilde{c}_{n+10} \tilde{d}_{n+23} \tilde{f}_{n+10} f_{n+14} \tilde{f}_{n+2} (\tilde{d}_{n+15} \tilde{e}_{n+3}) \tilde{c}_{n+2} c_{n+14} d_{n+1} e_{n+13} \tilde{e}_{n+11}) \\
&e_n \longmapsto (a_n b_{n+11} c_n d_{n+11} f_n \tilde{f}_{n+20} f_{n+8}) \\
&f_n \longmapsto ((\tilde{b}_n \tilde{c}_{n+11} \tilde{d}_n \tilde{f}_{n+11} f_{n+15} \tilde{f}_{n+3} \tilde{d}_{n+16})((c_{n+23} d_{n+10} f_{n+23} \tilde{f}_{n+19} f_{n+7})(\tilde{d}_{n+8} \tilde{e}_{n+20} e_{n+22})) \\
&) \longmapsto) \\
&(\longmapsto (
\end{aligned} \tag{6}$$

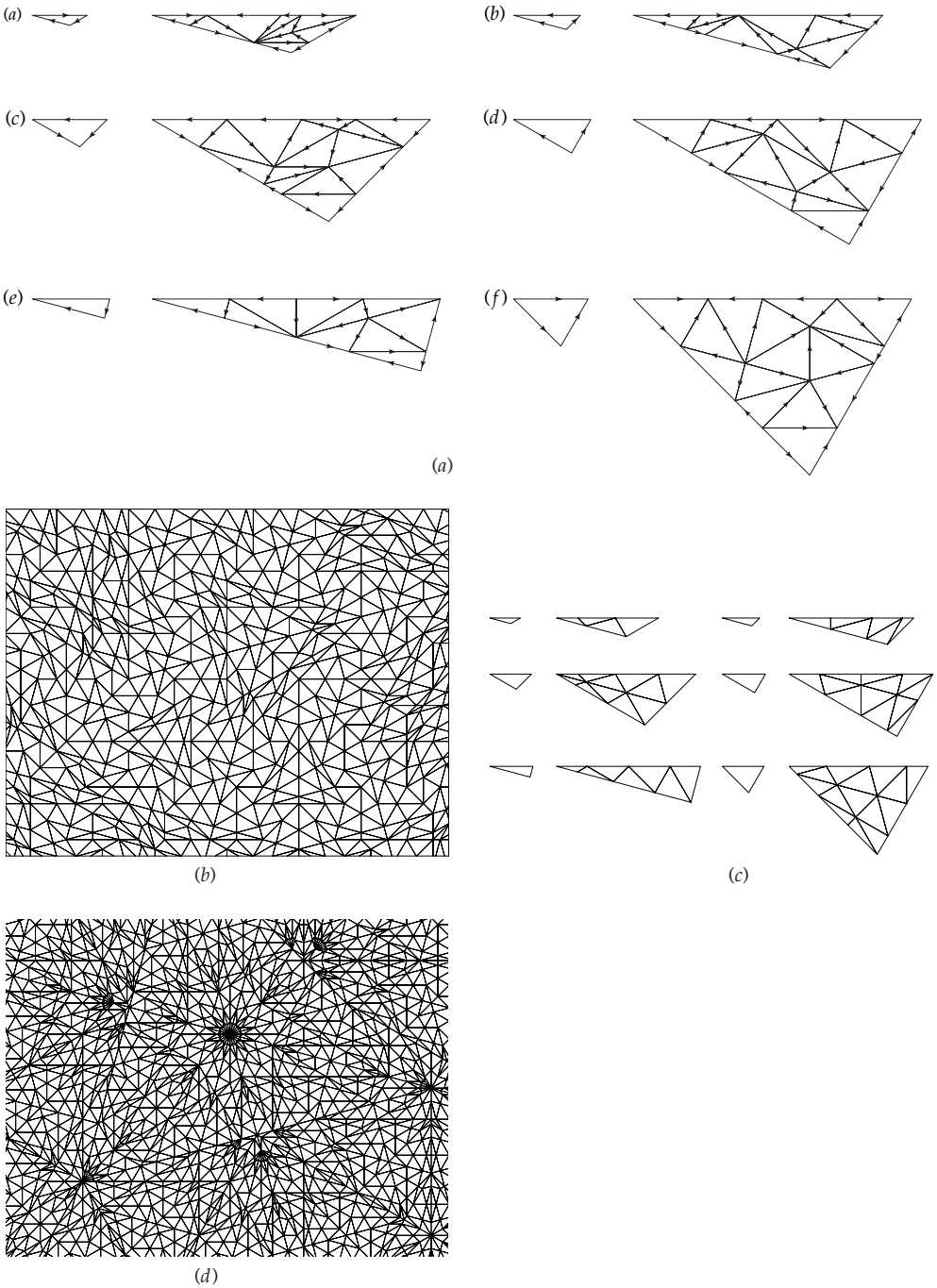

Figure 3. The patterns Til(12a) and Til(12b). (a) Substitution rules for Til(12a). (b) A portion of Til(12a). (c) Even iterations of these rules produce Til(12b). (d) A part of Til(12b).

By applying the inflation rules $\Psi_b(t_i) = \Phi_b^2(t_i)$, we obtain the patterns Til(12b). A part of the pattern, which is also face to face, can be seen in figure 3(d). The inflation factor is now the

Pisot number $(s_4/s_1)^2$, highest root of $x^2 - 12x + 9$. The analysis of the vertex configurations for Til($12a$) and Til($12b$) shows that both exhibit 36 in the iteration levels $n = 5$ and $n = 4$, respectively.

The study of the Bragg spectra for one-dimensional substitution tilings made in [12] has been generalized to higher dimensions in [13, 14]. They show that, up to possible extinctions, a self-similar tiling will show Bragg peaks in their diffraction pattern if the scaling factor is a Pisot number. According to [14], three types of Bragg spectra can be distinguished. If the scaling factor is a unit (the product of the roots of its minimal polynomial is 1), then the Bragg spectrum is finitely generated. If it is an irrational algebraic integer but not a unit, which occurs in Til($12b$), Til($8, +$) and Til($8, -$), then the support of the Fourier transform is not a finitely generated module and the tilings are called limit-quasiperiodic. These types of structures seem to occur much less frequently in the literature [14]. When the scaling factor is a non-unit rational integer (see [9] for an example with six-fold symmetry) then the tiling is called limit-periodic and the Bragg spectrum is not finitely generated. In what follows we analyse Til($12a$) which has a unit Pisot number as inflation factor.

The Fourier transform of a mass distribution $\rho(\mathbf{x})$ placed inside every tile is defined as usual

$$\mathcal{F}(\rho(\mathbf{x})) = \hat{\rho}(\mathbf{q}) = \int \exp(-\mathrm{i}\mathbf{q}\mathbf{x})\rho(\mathbf{x})\,\mathrm{d}^2x. \tag{7}$$

The simplest model of a quasicrystal structure consists in placing delta-like scatterers on the vertex positions of a tiling. Recursion relations for the Fourier amplitudes can be derived along the lines of [13, 10] for 2D and [15] for 3D. The unit vectors $\mathbf{u}_k$, $0 \leqslant k \leqslant d-1$, are such that the angle between $\mathbf{u}_k$ and the positive x-axis is equal to $k\pi/d$ ($d = 12$ in this section and 8 in section 4). For generic atomic decorations in the substitution tilings with the Pisot number α as a scaling factor, the Bragg spectrum can be identified, with the set of those wave vectors $\mathbf{q}$ for which $\exp(\mathrm{i}\mathbf{q}\alpha^n l_w \mathbf{u}_k) \to 1$ for $w = A, C, E$ and $k = 0, 2, 4, 6, 8, 10$ or $w = B, D, F$ and $k = 1, 3, 5, 7, 9, 11$ where the values for k represent the possible edge orientations. This condition is satisfied if the wave vectors are of the form

$$\frac{\mathbf{q}}{2\pi} = 2\sum_{k=0}^{d-1} m_{2k}\mathbf{u}_{2k}, \tag{8}$$

where m_{2k} are integers and $d = 6$ in this case.

If we define the numbers

$$\begin{aligned} &A_{n+2} = 4A_{n+1} - A_n \\ &A_0 = 1, \qquad A_1 = 4, \end{aligned} \tag{9}$$

then by induction on n:

$$\alpha^{n+1} = A_n\alpha - A_{n-1}. \tag{10}$$

The general solution to the difference equation

$$A(n+2) = \quad 4A(n+1) - A(n) \tag{11}$$

is

$$R(n) = \quad ax_1^n + bx_2^n, \tag{12}$$

with a, b arbitrary constants to be determined by the initial conditions and $x_1 = \alpha$, x_2 are the roots of the polynomial $x^2 - 4x + 1$. Keeping in mind that x_2 is less than 1 in modulus:

$$\lim \frac{A_n}{A_{n-1}} = \alpha. \tag{13}$$

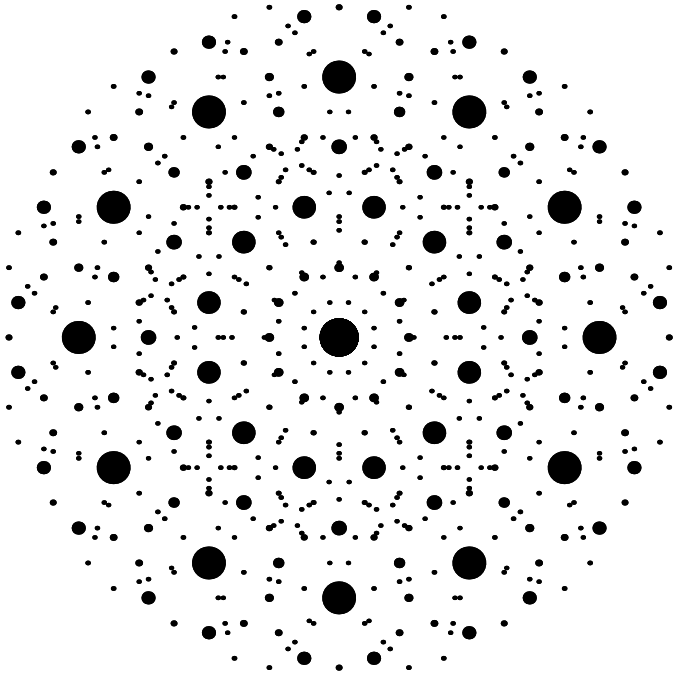

Figure 4. Diffraction image of Til(12a).

For a wave vector of the form given by equation (8), it can be checked that all the phases are integer multiples of 2π in the $n \to \infty$ limit by taking into account $\cos(\pi/12) = \theta/2, \cos(2\pi/12) = (\theta^2 - 2)/2, \cos(3\pi/12) = (\theta^3 - 2\theta)/2, \cos(4\pi/12) = (2\theta^2 + 1)/2, \cos(5\pi/12) = (4\theta - \theta^3)/2$, where $\theta^2 = \alpha$.

The diffraction pattern for Til(12a) can be seen in figure 4. In the figure the area of a disc is proportional to the intensity of the corresponding peak. It has been computed for an iteration level $n = 30$ (with a magnitude order of 10^{34} atomic positions). The cut-off is at 1.3% and $-5 \leqslant m_{2k} \leqslant 5$ and the pattern shows 12-fold symmetry.

4. Non-periodic patterns with two-fold and four-fold symmetries

A description of Til(−) and Til(+) in terms of Lindenmayer systems, along the lines of equation (4), is also possible [6]. The analysis of the permitted tile orientations, together with the type of the edge substitution rules, allows us to get them by superimposing structures with less orientations [11]. One of the structures of Til(−) can be converted into a face-to-face pattern Til(2). The tiling Til(4) is obtained by changing the prototile shapes of one of the substructures in Til(+). The pattern Til(2) has eight prototiles (table 3) $p(X, Y, \ldots, Z)$ which are obtained by concatenating the edges $X, Y, \ldots, Z$ in anticlockwise orientation by starting with the edge X in the horizontal position shared with its inflated version (see figure 5(a)). The edge lengths are $[A] = \sin(\pi/8), [C] = \sin(3\pi/8), [G] = [A], [R] = [F] = [C], [E] = [M] = [C] + [A], [H] = [K] = 2[C]$. The edge X_m^k is obtained by a rotation of $(m-1)\pi/d$ of X_1^k ($d = 4$ in this section and $d = 6$ in section 5). The vertex $X \cap Z$ of $p(X, Y, \ldots, Z)$ is placed in the origin and the edge X on $\mathbf{u}_0$. The edge substitution rules are given in table 3.

Table 3. Prototiles and edge inflation rules for Til(2) and Til(4) (see figures 5 and 6).

Til(2)		
Tiles		
a	b	c
$\mathrm{p}(C_1^1, A_3^0, C_1^1, A_3^0)$	$\mathrm{p}(R_1^0, E_3^0, C_2^0, A_4^1, F_3^1)$	$\mathrm{p}(H_1, M_4^0, E_2^0)$
d	e	f
$\mathrm{p}(E_1^0, A_2^0, C_4^1, A_2^0, C_4^1, M_3^0)$	$\mathrm{p}(F_1^1, G_3^0, A_4^0, C_2^1)$	$\mathrm{p}(H_1, G_4^1, F_2^0, C_1^0, A_3^1, K_2)$
g	h	
$\mathrm{p}(H_1, G_4^1, F_2^0, C_1^0, A_3^1, A_1^0, C_3^1, E_2^1, R_4^1, F_2^0)$	$\mathrm{p}(H_1, F_4^1, G_2^0, H_1, F_4^1, G_2^0)$	
Edge inflation rules		
A^0	C^0	E^0
C^0	HA^0	$R^1R^0M^1$
F^0	G^0	H
R^0M^1	F^0	HA^0A^1H
K	M^0	R^0
$M^0R^1R^0M^1$	KE^1	F^0E^1

Til(4)		
Tiles		
a	$\bar{a}$	b
$\mathrm{p}(Q_1^0, C_3^0, T_4^0, C_3^0, T_2^0)$	$\mathrm{p}(R_1^1, T_3^1, C_4^1, T_3^1, C_2^1)$	$\mathrm{p}(P_1, Q_4^1, Q_2^1)$
c	d	e
$\mathrm{p}(C_1^0, A_4^0, S_1^0, A_2^0)$	$\mathrm{p}(P_1, C_4^0, T_1^0, A_3^1, S_2^1)$	$\mathrm{p}(T_1^0, C_4^0, S_2^1, A_3^1)$
$\bar{e}$	f	g
$\mathrm{p}(T_1^1, C_4^1, S_2^0, A_3^0)$	$\mathrm{p}(Q_1^0, T_4^1, C_1^1, A_4^1, S_3^1)$	$\mathrm{p}(Q_1^0, R_4^1, S_1^0, A_2^0, A_4^1, S_3^1)$
h	k	l
$\mathrm{p}(T_1^0, A_3^1, T_1^0, A_3^1)$	$\mathrm{p}(Q_1^0, C_3^0, C_1^1, A_4^1, T_2^0)$	$\mathrm{p}(P_1, S_4^0, C_2^1, T_1^1, C_4^1, T_3^1, C_2^1)$
m		
$\mathrm{p}(C_1^1, T_4^1, A_2^0, C_1^0, A_2^0, T_4^1)$		
Edge inflation rules		
A^0	S^0	C^0
C^1	T^1	PA^1
T^0	R^0	Q^0
C^1Q^0	$C^0C^1Q^0$	PR^0
P		
$Q^1C^0C^1Q^0$		

If we represent an eight-fold rotation around the origin by $\zeta^2 = \exp(\mathrm{i}2\pi/8)$, a translation along the vector $\mathbf{u}_k$ by ζ^k, and a rotation r followed by a translation t by $[r, t]$, then the pattern x_n, obtained by applying n times the substitution rules given in figure 5(a) to the tile x, can be described in the following way:

$$a_n = [\zeta^6, \alpha^n\zeta^2]\widetilde{e}_{n-1} \cup [1, \alpha^{n-1}]h_{n-1} \cup [\zeta^{14}, \alpha^{n+1}]\widetilde{e}_{n-1}$$

$$b_n = [\zeta^{12}, 0]\widetilde{b}_{n-1} \cup [\zeta^{10}, \alpha^{n-1}(\zeta^3+\alpha)]\widetilde{a}_{n-1} \cup [\zeta^4, \alpha^n(\zeta^4+\alpha)](b_{n-1}+\widetilde{b}_{n-1})$$
$$\cup [\zeta^{10}, \alpha^n((\alpha+1)\zeta^2 - 2\zeta + \alpha)]\widetilde{c}_{n-1} \cup [1, \alpha^n\zeta^2]d_{n-1}$$

$$c_n = [\zeta^{10}, 0]\widetilde{e}_n \cup [\zeta^6, \alpha^n(\zeta^2+\alpha)]\widetilde{e}_{n-1} \cup [1, 2\alpha^{n+1}]\widetilde{f}_{n-1} \cup [\zeta^{10}, \alpha^{n+1}\zeta]b_{n-1}$$
$$\cup [1, \alpha^n(\zeta^2 + (1+\alpha))]\widetilde{a}_{n-1}$$

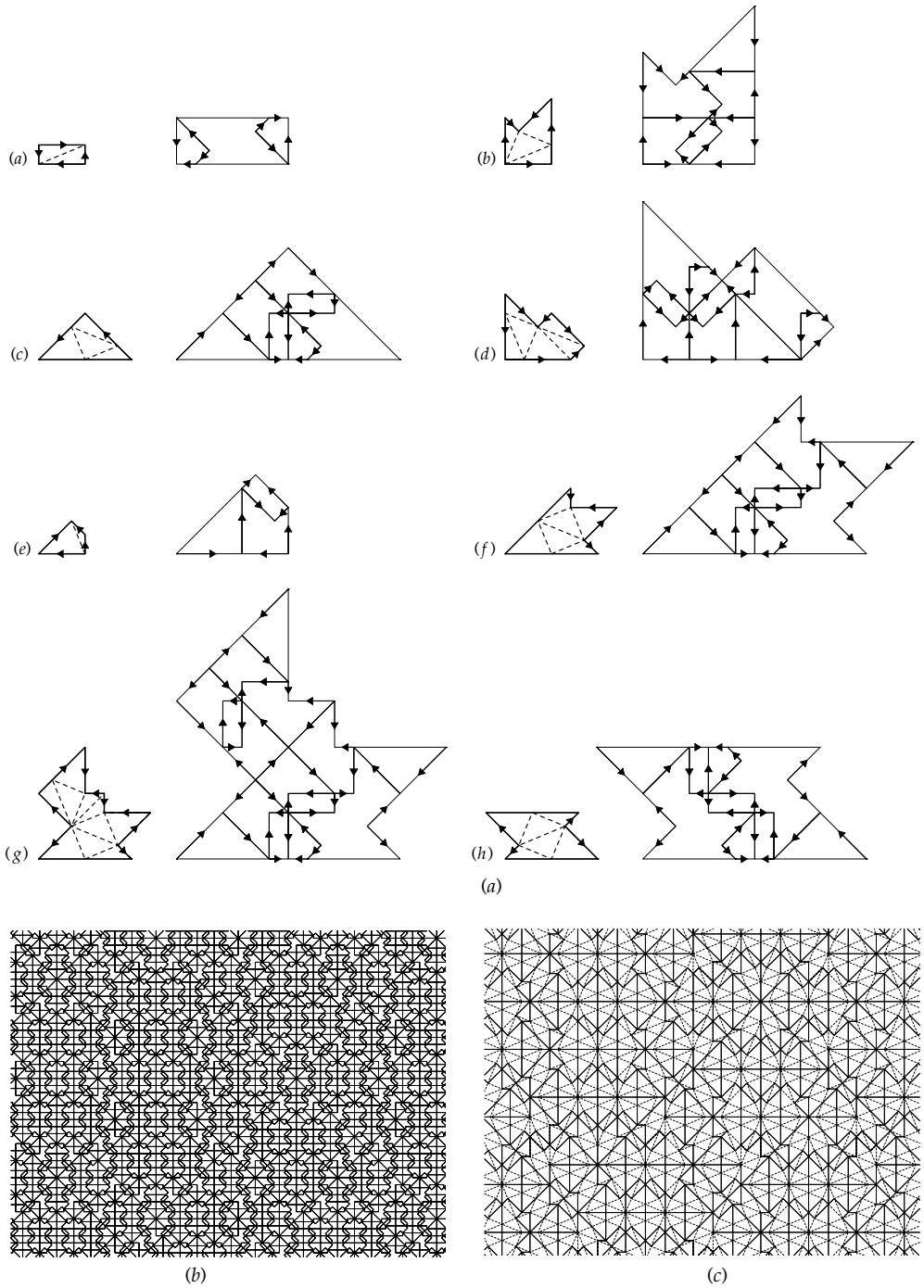

Figure 5. The pattern Til(2). (*a*) Substitution rules for the tiles with edges given in table 3. The first inflation step is shown in the figure. It corresponds to $n = 1$ in equation (14) which gives the prototiles translations and rotations necessary to generate the inflated tiles. (*b*) A portion of Til(2). (*c*) Triangle pattern obtained from Til(2).

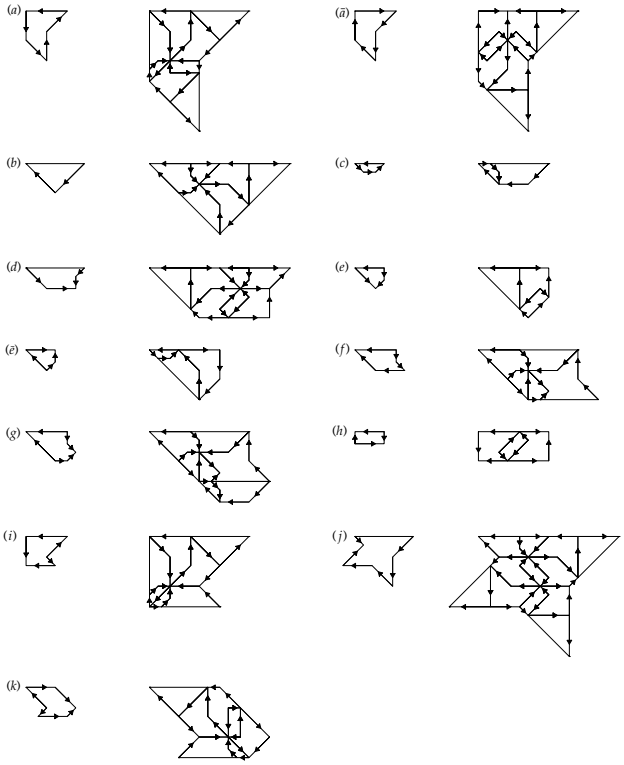

(*a*)

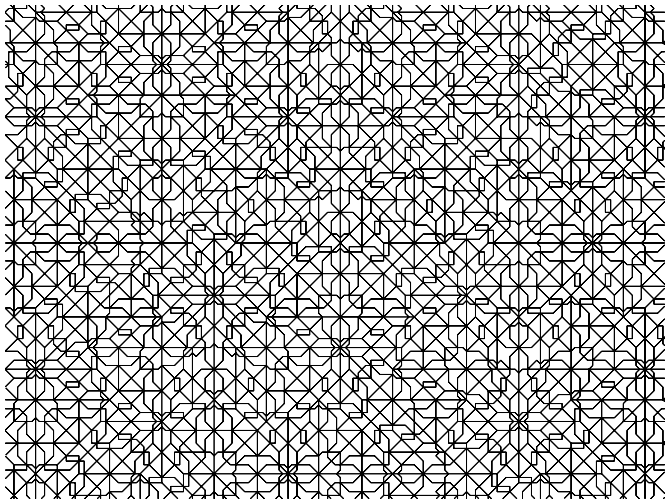

(*b*)

Figure 6. The pattern Til(4). (*a*) Substitution rules. (*b*) A portion of Til(4).

$$d_n = [\zeta^6, \alpha^n(1+\alpha)]c_n \cup [\zeta, \alpha^n(\alpha\zeta + 1 + \alpha)]\widetilde{a}_n$$

$$e_n = [1, \alpha^{n+1}]\widetilde{b}_{n-1} \cup [\zeta^{10}, 2\alpha^n\zeta]c_{n-1} \cup [\zeta^6, \alpha^{n+1}\zeta]\widetilde{a}_{n-1}$$

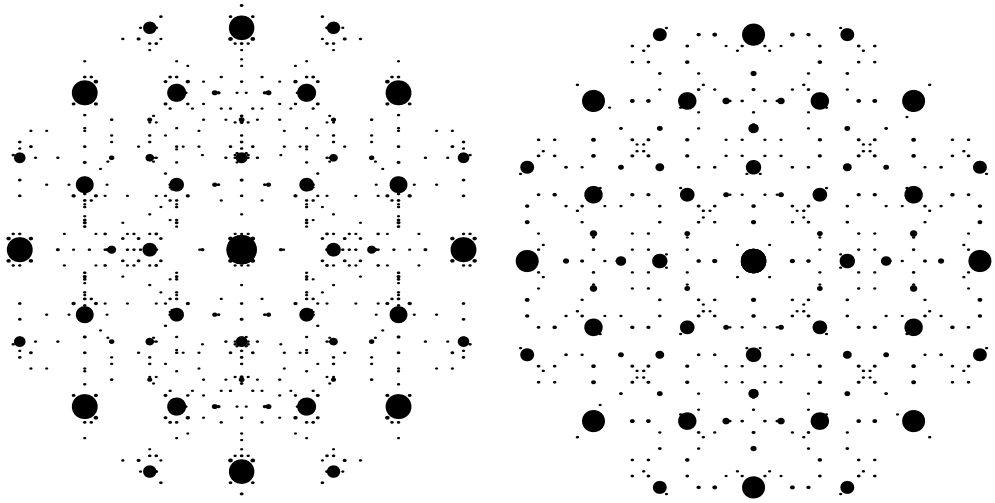

(*a*) (*b*)

Figure 7. Diffraction images of (*a*) Til(2) and (*b*) Til(4).

$$
\begin{aligned}
f_n = {} & [\zeta^{10}, 0]\tilde{e}_n \cup [\zeta^6, \alpha^n(\zeta^2+\alpha)]\widetilde{e}_{n-1} \cup [1, 2\alpha^{n+1}]\widetilde{g}_{n-1} \\
& \cup [\zeta^8, \alpha^{n-1}(-\alpha\zeta^2 + 2\alpha^2\zeta + 1)]\widetilde{c}_{n-1} \\
& \cup [\zeta^{14}, \alpha^n(1+\alpha)\zeta]d_{n-1} \cup [\zeta^{10}, \alpha^{n+1}\zeta]\widetilde{b}_{n-1} \\
& \cup [\zeta^8, \alpha^{n-1}(-\alpha\zeta^3 + \zeta^2 + \alpha^2\zeta)]\widetilde{a}_{n-1} \\
g_n = {} & f_n \cup [\zeta^{14}, \alpha^{n+1}\zeta^3]\widetilde{b}_n \\
h_n = {} & g_{n-1} \cup [\zeta^{10}, \alpha^n(\zeta^2+\alpha)]e_{n-1} \cup [\zeta^{12}, \alpha^{n+1}]\widetilde{a}_{n-1} \cup [1, 2\alpha^{n-1}(1+\alpha)]c_{n-1} \\
& \cup [\zeta^8, \alpha^n(\alpha\zeta^3 + \zeta + 2\alpha)]g_{n-1} \cup [\zeta, \alpha^n(\alpha\zeta^3 - \zeta^2 + \zeta + \alpha)]e_{n-1} \\
& \cup [\zeta^2, \alpha^n(\alpha\zeta^3 + \zeta + \alpha)]\widetilde{a}_{n-1} \cup [\zeta^8, \alpha^n(\alpha\zeta^3 + \zeta + 2)]c_{n-1} \\
& \cup [1, \alpha^{n-1}(\alpha^2\zeta^3 - (1+\alpha)\zeta^2 + \alpha\zeta + \alpha^2)]a_{n-1}
\end{aligned}
\tag{14}
$$

where $\alpha = \sin(3\pi/8)/\sin(\pi/8)$ is the tilings inflation factor and $[A] = 1, [C] = \alpha$ for simplicity. A portion of the tiling can be seen in figure 5(*b*). By marking with straight line segments the prototiles interiors as in figure 5(*a*), we can get a pattern with the same prototiles appearing in Til(8, −) (figure 5(*c*)).

The prototiles (figure 6(*a*)) and edge inflation rules for the pattern Til(4) are described in table 3. where $[S] = [A], [T] = [C], [Q] = [C] + [A], [P] = 2[C]$. The tile inflation rules can be seen in figure 6(*a*) and a portion of the pattern in figure 6(*b*). In Til(2), the 23 vertex configurations appearing in the fourth iteration level coincide with those appearing in the fifth level. The 70 vertex configurations for Til(4) appear in the sixth iteration level.

In figures 7(*a*) and (*b*), we can see the Fourier intensities for Til(2) and Til(4), respectively. They have been computed along the lines of [13, 10] by using recursion relations between Fourier amplitudes derived from equation (14) (and analogous equation for Til(4)). The Bragg peaks are given by equation (8) with $d = 4$. The computed diffraction patterns (figure 7) correspond to c_{12} for Til(2) (7 804 510 563 atomic positions) and b_{12} for Til(4) (8 095 487 406

Table 4. Prototiles and edge inflation rules for Til(6, −) and Til(6, +) (see figures 8 and 9).

Til(6, −)		
Tiles		
a	b	c
$\mathrm{p}(E_1^1, A_4^1, K_6^0, C_3^0)$	$\mathrm{p}(H_1^0, G_6, L_4^1)$	$\mathrm{p}(L_1^1, P_4^0, C_1^0, A_6^0, E_3^0)$
d	e	f
$\mathrm{p}(G_1, C_5^1, K_2^1, G_1, C_5^1, K_2^1)$	$\mathrm{p}(M_1, A_6^0, E_3^0, C_1^1, K_4^0, G_3)$	$\mathrm{p}(C_1^1, P_4^1, L_1^0, E_5^0, A_2^1, A_6^0)$
g		
$\mathrm{p}(H_1^0, E_6^1, A_3^1, K_5^0, C_2^0, L_4^1)$		
Edge inflation rules		
A^0	C^0	E^0
E^1	P^1H^0	$A^1H^1H^0$
K^0	P^0	L^0
GC^1	L^0GC^1	$P^0P^1H^0$
G	H^0	M
$H^1H^0A^0A^1H^1H^0$	L^0GMG	$H^1P^0P^1H^0$

Til(6+)		
Tiles		
a	b	c
$\mathrm{p}(K_1^0, P_6^0, P_2^0)$	$\mathrm{p}(F_1^1, A_4^1, F_1^1, A_4^1)$	$\mathrm{p}(C_1^1, L_4^1, C_1^1, L_4^1)$
d	e	f
$\mathrm{p}(F_1^0, A_4^0, T_5^0, E_2^0)$	$\mathrm{p}(N_1, P_5^1, K_2^0)$	$\mathrm{p}(L_1^0, E_5^1, T_2^1, C_2^0)$
g	h	i
$\mathrm{p}(K_1^0, F_6^0, A_3^0, E_1^1, C_4^1)$	$\mathrm{p}(K_1^0, C_6^0, L_3^0, K_1^1, E_5^1, T_2^1)$	$\mathrm{p}(M_1, C_6^0, E_3^0, C_2^0, L_5^0, K_2^1)$
j	k	l
$\mathrm{p}(K_1^1, K_5^1, K_3^1)$	$\mathrm{p}(C_1^0, E_4^0, C_3^0, E_6^0, P_5^0)$	$\mathrm{p}(N_1, T_5^0, E_2^0, F_1^0, A_4^0, M_2)$
m	n	
$\mathrm{p}(C_1^1, K_2^1, K_6^1, E_4^1, C_1^1, L_4^1)$	$\mathrm{p}(F_1^1, A_4^1, F_1^1, P_5^1, K_2^0, A_4^1)$	
o		
$\mathrm{p}(N_1, T_5^0, E_2^0, F_1^0, A_4^0, C_1^0, E_4^0, P_3^0, C_5^0, E_2^0)$		
p		
$\mathrm{p}(E_1^1, C_4^1, K_1^0, F_6^0, A_3^0, C_6^0, E_3^0, C_2^0, L_5^0, K_3^1)$		
Edge inflation rules		
A^0	T^0	C^0
F^1	E^1	K^0E^1
L^0	E^0	F^0
C^1N	C^1NP^0	$K^0K^1A^1$
P^0	M	N
K^0M	$P^1NC^0C^1NP^0$	$K^0K^1A^1A^0K^0K^1$
K^0		
$NC^0C^1NP^0$		

atomic positions). The cut-off is at 2.2% of the central intensity and $-7 \leqslant m_{2k} \leqslant 7$. The rings with apparent octagonal symmetry are formed by rotated copies of rings with lower symmetry. Two-fold and four-fold are the exact symmetries of the patterns which are shown in the diffraction images.

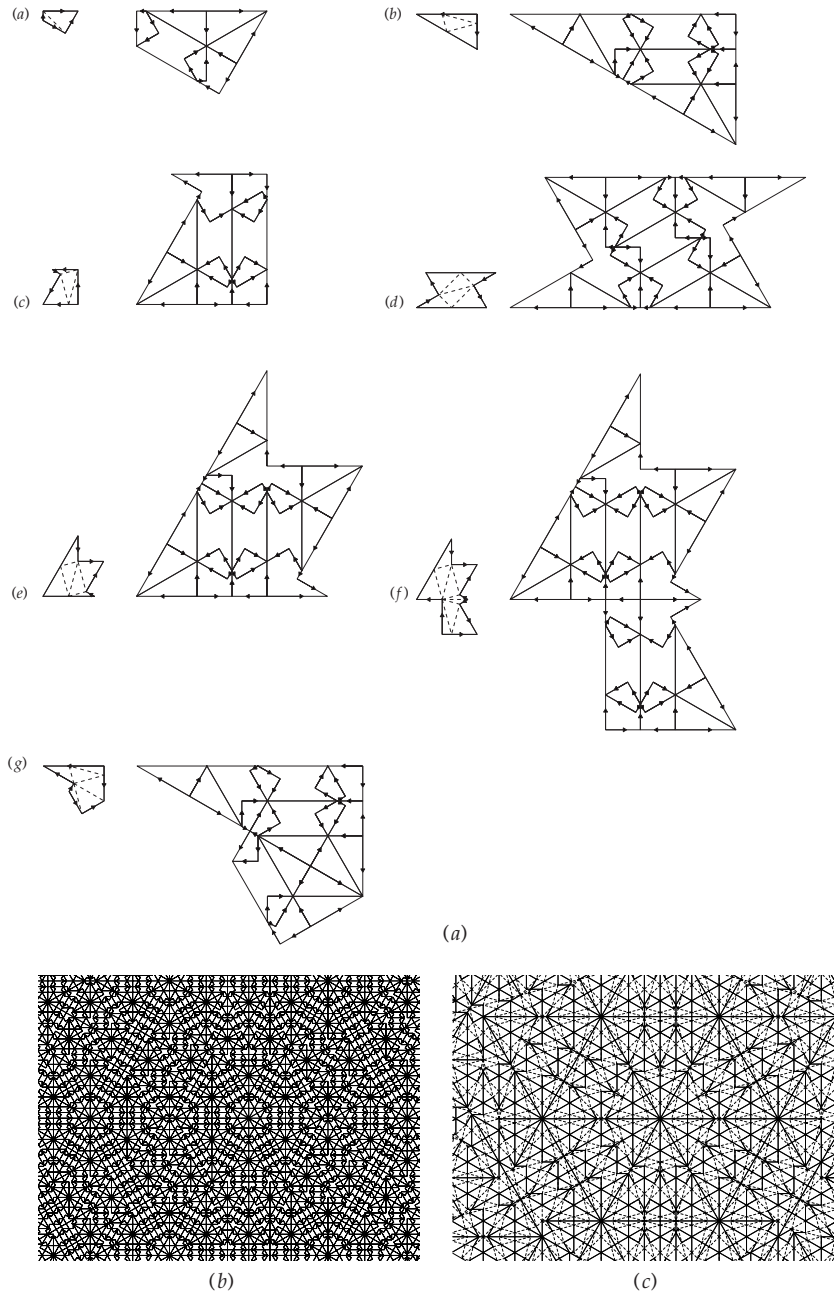

Figure 8. The pattern Til(6, −). (*a*) Substitution rules. (*b*) A portion of Til(6, −). (*c*) Triangle pattern obtained from Til(6, −).

5. Hexagonal non-periodic patterns

Two types of triangle patterns Til(12, −) and Til(12, +) with the Pisot inflation factor $\sin(3\pi/12)/\sin(\pi/12)$ were introduced in [8]. Their grammar description allows us to

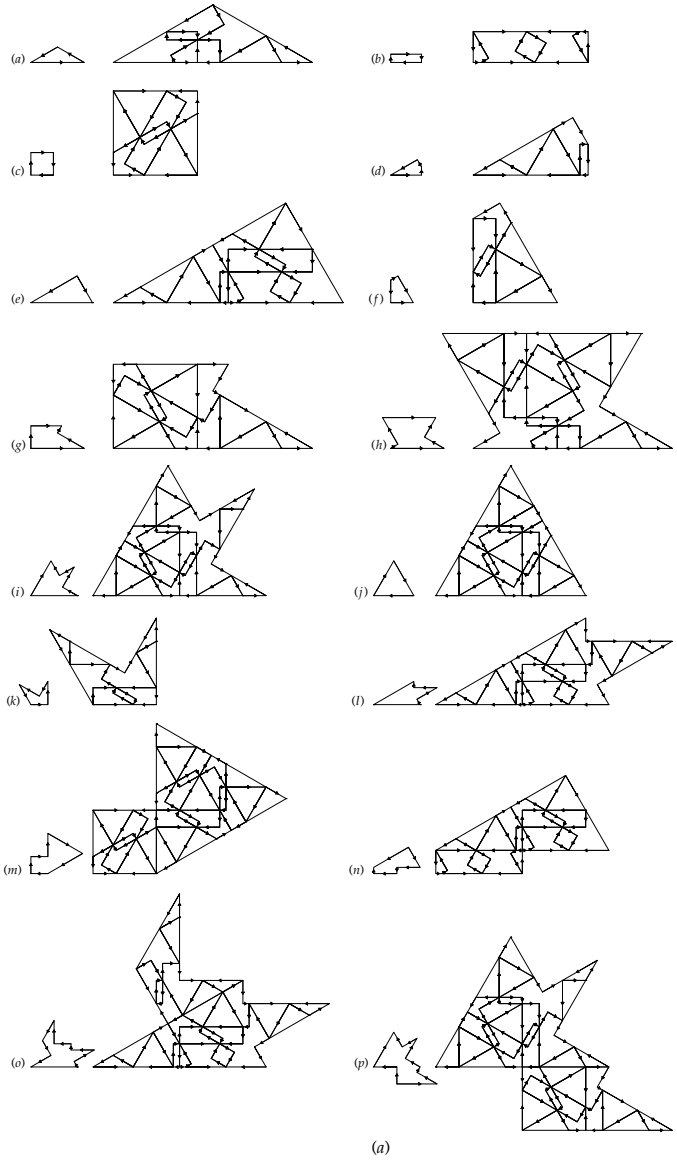

Figure 9. The pattern Til(6, +). (*a*) Substitution rules. (*b*) A portion of Til(6, +).

compute the tile orientations in an efficient way. This information and the type of edge inflation rules are necessary in order to get subpatterns with half the orientations. One of the subpatterns for each original pattern can be converted into face-to-face patterns. We denote the transformed subpatterns by Til(6, −) and Til(6, +). In this section, we study their inflation rules and diffraction properties. In table 4, we show the prototiles (figure 8(*a*)) and substitution rules for the edges for Til(6, −). The edge lengths are $[A] = \sin(\pi/12)$, $[C] = \sin(3\pi/12)$, $[E] = \sin(5\pi/12)$, $[K] = [C]$, $[L] = [P] = [E]$, $[H] = [C] + [E]$, $[G] = 2[E]$, $[M] = 2[C]$.

A portion of Til(6, −) can be seen in figure 8(*b*). It is possible to mark the prototile interiors by straight line segments (figure 8(*a*)) and we obtain a pattern (figure 8(*c*)) with the

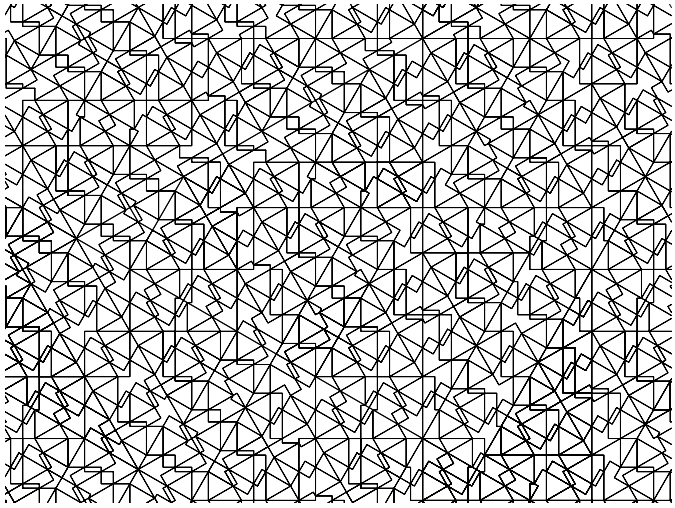

(*b*)

Figure 9. (Continued.)

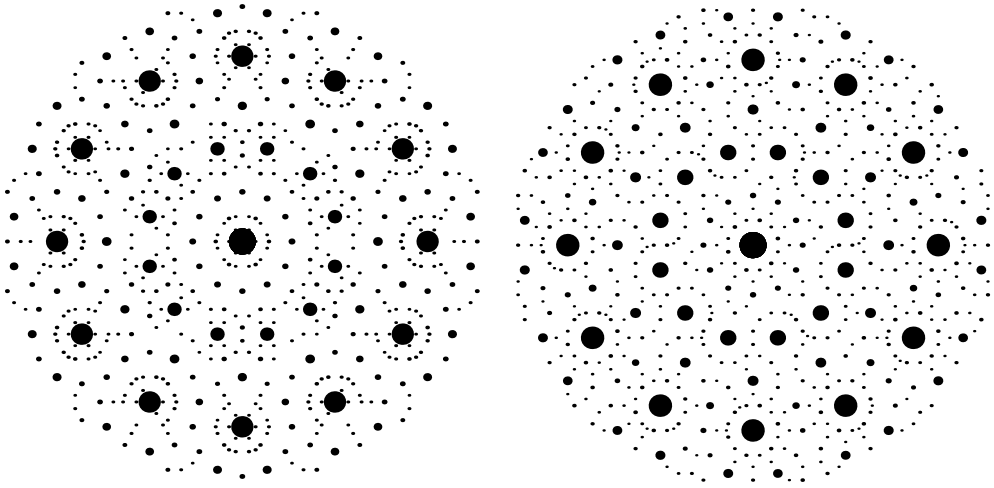

(*a*) (*b*)

Figure 10. Diffraction images of (*a*) Til(6, −) and (*b*) Til(6, +).

same prototiles as Til(12*a*). The prototiles (figure 9(*a*)) for Til(6, +) and edge inflation rules are given in table 4 where $[T] = [A]$, $[L] = [C]$, $[F] = [E]$, $[P] = [C] + [A]$, $[M] = [N] = 2[E]$, $[K] = [C] + [E]$. A characteristic distinguishing this pattern (figure 9(*b*)) is that it contains only rotated prototiles while the other patterns studied in this work have both rotated and reflected prototiles. The number of vertex configurations in the third and fourth iteration levels is 29 for Til(6, −). The 48 vertex configurations in Til(6, +) appear in the fourth level.

The diffraction images for the pattern b_9 of Til(6, −) (60 475 606 682 atomic positions) and j_8 of Til(6, +) (9 142 055 988 atomic positions) can be seen in figures 10(*a*) and (*b*) respectively. Bragg peaks are indexed as equation (8) for $d = 6$. The cut-off is at 4.3%

for Til(6, −) and 2.8% for Til(6, +) of the central intensity and $-5 \leqslant m_{2k} \leqslant 5$. While the peaks with highest intensities are situated in apparent dodecagonal rings, their symmetries are hexagonal.

6. Conclusion

The main purpose of this paper has been the generation by means of inflation rules of several patterns which are non-periodic. They show non-crystallographic and crystallographic symmetries. Aperiodic tetragonal patterns have been derived in [16] and several dodecagonal patterns have been given in [17–19]. In the dodecagonal pattern derived in [17] the Bragg positions are 12-fold symmetric, whereas the intensities of the Bragg peaks are only six-fold symmetric [14]. Non-periodic square–triangle tilings with hexagonal symmetries are described in [20]. Also limit-quasiperiodic square–rhombus patterns with octagonal symmetry were derived in [21]. In comparison with the patterns having the same symmetries appearing in the cited literature, the patterns presented in this work show a higher number of vertex configurations. This is specially evident for the limit-quasiperiodic pattern Til(8, +). In the case of the transformed patterns, the prototile boundaries are more complex than normally and the exact symmetries appear in Bragg peaks with lower intensities. Low resolution of the diffraction images shows apparent octagonal and dodecagonal symmetries. These peaks are in fact situated within rotated rings with lower symmetries and a small difference in their intensities.

In [22], phase transformations in the octagonal ternary alloy of Mn–Si–Al have been considered. Octagonal–cubic phase transitions have been observed by transmission electron microscopic observations. Electron diffraction patterns show intermediate phases during the phase transitions. In addition to the common use of large unit cells of approximants, the tilings presented in this work could be considered in order to describe intermediate structures in octagonal–cubic and dodecagonal–hexagonal phase transitions.

The generation of the tilings by projection methods [3, 23], the existence of matching rules [24] and the search of a minimal prototile set are open questions which must also be studied.

References

[1] Shechtman D, Blech I, Gratias D and Cahn J W 1984 Metallic phase with long-range orientational order and no translational symmetry *Phys. Rev. Lett.* **59** 1951–3
[2] Ishimasa T, Nissen H U and Fukano Y 1985 New ordered state between crystalline and amorphous in Ni–Cr particles *Phys. Rev. Lett.* **55** 511–3
[3] Kramer P and Neri R 1984 On periodic and non periodic space fillings of E^n obtained by projection *Acta Cryst.* A **40** 580–7
[4] Nissen H U and Beeli C 1993 Electron microscopy of quasicrystals and the validity of the tiling approach *Int. J. Mod. Phys.* B **7** 1387–413
[5] Nischke K P and Danzer L 1996 A construction of inflation rules based on *n*-fold symmetry *Discrete Comput. Geom.* **15** 221–36
[6] Escudero J G 2000 Stochastic L-systems and quasicrystal patterns *Mater. Sci. Eng.* A **294–296** 388–91
[7] Escudero J G 2001 Deterministic and non deterministic quasicrystal patterns with even symmetries *Ferroelectrics* **250** 327–30
[8] Escudero J G 2001 ET0L-systems for composite dodecagonal quasicrystal patterns *Int. J. Mod. Phys.* B **15** 1165–75
[9] Escudero J G 2004 Configurational entropy for stone-inflation hexagonal and octagonal patterns *Int. J. Mod. Phys.* B **18** 1595–602
[10] Escudero J G and Garcia J G 2001 Simple and composite octagonal quasicrystal patterns *J. Phys. Soc. Japan* **70** 3511–6

[11] Escudero J G and Garcia J G 2002 Hierarchies of quasicrystal substitutional patterns *J. Alloys Compounds* **342** 203–5
[12] Bombieri E and Taylor J E 1986 Which distributions of matter diffract? *J. Phys. France Coll.* C **3** 19–28
[13] Godreche C and Luck J M 1989 Quasiperiodicity and randomness in tilings of the plane *J. Stat. Phys.* **55** 1–28
[14] Gaehler F and Klitzing R 1997 The diffraction pattern of selfsimilar tilings *Proc. NATO ASI The Mathematical Foundations of Long Range: Aperiodic Order* (Dordrecht: Kluwer) 141–74
[15] Escudero J G and Garcia J G 2003 Diffraction on icosahedral Danzer tilings *Mod. Phys. Lett.* B **17** 303–9
[16] Lifschitz R 2002 The square Fibonacci tiling *J. Alloys Compounds* **342** 186–90
[17] Stampfli P 1986 A dodecagonal quasiperiodic lattice in two dimensions *Helv. Phys. Acta* **59** 1260–2
[18] Gaehler F and Rhyner J 1986 Equivalence of the generalised grid and projection methods for the construction of quasiperiodic tilings *J. Phys. A: Math. Gen.* **19** 267–77
[19] Niizeki K and Mitani H 1987 Two-dimensional dodecagonal quasilattices *J. Phys. A: Math. Gen.* **20** L405–10
[20] Paredes R, Aragon J L and Barrio R A 1998 Nonperiodc hexagonal square–triangle tilings *Phys. Rev.* B **58** 11990–5
[21] Watanabe Y, Ito M and Soma T 1987 Nonperiodic tessellation with eightfold rotational symmetry *Acta. Cryst.* A **43** 133–4
[22] Xu L, Wang N, Lee S T and Fung K K 2000 Electron diffraction study of octagonal–cubic phase transitions in Mn–Si–Al *Phys. Rev.* B **62** 3078–82
[23] Duneau M and Katz A 1985 Quasiperiodic patterns *Phys. Rev. Lett.* **54** 2688–91
[24] Goodman-Strauss C 1998 Matching rules and substitution tilings *Ann. Math.* **147** 181–223